Quantum Physics Letters
An International Journal

http://dx.doi.org/10.18576/qpl/050202

Real Cluster Folding Potential for α+^{40}Ca Elastic Scattering

Zakaria M. M. Mahmoud[1,2] *and Kassem. O. Behairy*[3,*]

[1]Physics Department, Faculty of Science, Assiut University, New Valley Branch, Egypt.
[2]Physics Department, Philipps University Marburg, D-35032 Marburg, Germany
[3]Physics Department, Aswan University, Aswan, Egypt.

Received: 21 Jun. 2016, Revised: 22 Jul. 2016, Accepted: 24 Jul. 2016.
Published online: 1 Aug. 2016.

Abstract: elastic scattering of α+^{40}Ca are analyzed in the framework of optical model based on the α-cluster model of ^{40}Ca. We adopted an independent α-cluster model to generate the α-cluster and matter densities of ^{40}Ca. we pre-suggested the functional form of α-cluster density and fixed its parameters according to the available experimental data about the α-particle and ^{40}Ca nuclei. The obtained α-cluster density of ^{40}Ca is used to generate the real part of the optical potential. The single folding procedure is used to generate this real optical potential with two different effective α-α interactions. The real calculated potential supplied with an imaginary squared Woods Saxon potential are used to analyze 20 sets of experimental data on the energy range between 18 and 166 MeV. We found that our model is successful in reproducing the data for energies above 40 MeV and still doubtful for lower energies.

Keywords: Optical potential model, single folding, cluster model, α+40Ca elastic scattering.

1 Introduction

Collision between nuclear species is considered as a powerful way to get information about nuclear interaction potential and nuclear density. The simplest nuclear collision process which is considered as the doorway for other reactions is the elastic scattering. Optical model is one of the mostly used models for the description of nuclear scattering especially elastic scattering. The microscopic description of the nucleus–nucleus optical model potential is considered as one of the fundamental tasks in nuclear physics. Good microscopic understanding of this potential allows, besides understanding the relevant reaction dynamics involved, predicting optical potentials of colliding systems for which the elastic scattering measurement is absent. One of the mostly used methods to calculate the nucleus-nucleus interaction potential is the folding model. Folding formulation of the nucleus–nucleus potential was pioneered by Watanabe [1] in his analysis of deuteron projectiles.

Through the last few decades folding model calculations was used for the analysis of scattering processes for a large number of interacting systems with microscopic and semi-microscopic approaches. Successfully and intensively Satchler and Love [2] used double folding (DF) model for the analysis of light and heavy composite ions scattering. They used in their analysis DF optical potentials built upon a realistic effective nucleon–nucleon interaction folded with the nuclear matter density distributions of projectile and target nuclei. It is appeared that the beauty of the folding model lies in its abilities to relate the nuclear potential to some fundamental quantities, namely nuclear densities and nucleon-nucleon effective interactions. More review of this subject can be found in ref. [3].

The DF model based on the point nucleon densities and an effective nucleon-nucleon interaction is widely and successfully used to analyze α-nucleus and nucleus-nucleus elastic scattering [4-9]. Also another approach of the folding model based on α-cluster picture of the nucleus is used. This α-cluster based folded potential is used to analyze the elastic scattering of α-particle and α-like nuclei from other α-like nuclei [10-13]. This α-cluster picture dated back to the beginning of nuclear physics through the explanation of nuclear α-decay from heavy nuclei. For more details and review about α-clustering in light nuclei from both experimental and theoretical point of view see ref. [14,15] and references therein.

Previously, the present α-cluster folding model was used successfully to describe the α-nucleus [16] and nucleus–nucleus scattering [17]. The interaction potentials between

*Corresponding author e-mail: kass_phys@aswu.edu.eg

these systems are formulated through the folding procedures built upon an appropriate effective α–α interaction folded over the α-cluster density distribution of the target nucleus. Recently the α-cluster folding model is applied successfully to analyze the diffractive elastic scattering of $^{12}C+^{12}C$ [18], $^{16}O+^{16}O$ [19] and elastic, inelastic and fusion reactions of $^{12}C+^{24}Mg$ [20] systems.

The α-cluster folding model has two important ingredients α-cluster density of the target and an appropriate effective α-α interaction. The α-α effective interaction could be treated both phenomenologically [21-23] or microscopically [24-27]. The parameters of these interactions can be adjusted to fit some experimental data as the energy and the decay width of the virtual ^{8}Be nucleus or the elastic scattering phase shifts of α–α system itself.

In the present work, the singe folding α-cluster (SFC) model is used to generate $\alpha+^{40}Ca$ real part of the optical potentials. A simple α-cluster model is used to get the α-cluster density of the target nuclei. This model is based in our previous work found in ref. [16]. The new in this work is that we pre-suggested the α-cluster density profile of the target nuclei. This form respects the exponential decay of the point nucleon matter density distribution at the nucleus surface. The parameters of this suggested form is fixed according to our experimental information of the α-particle and the target nuclei. So, the aim in this work is to obtain a continuous α-cluster distribution inside the nucleus in model independent way. Hopefully this α-cluster distribution is closed to the expected α-cluster distribution inside the nucleus. To validate this model, it is used to analyze the elastic scattering data of the $\alpha+^{40}Ca$ system over a wide range of energies and angular distribution. The ^{40}Ca nucleus is chosen because *1-)* the scattering of α from it is characterized by large angle scattering anomaly (LASA) for energy less than 55 MeV and Nuclear rainbow for energies above 100 MeV *2-)* the availability of enormous sets of experimental data over a wide energy range cover both this scattering phenomena. These two phenomena reflect the transparency of the potential over a wide radial domain so with them a potential free of ambiguities could be obtained. For this reasons this system is a good test for any theoretical model. For this purpose the obtained density in this work is implemented in the single folding (SF) formula with an appropriate α-α effective interaction to obtain the α-nucleus real potential. The calculated SF cluster potential is used to analyze twenty sets of $\alpha+^{40}Ca$ elastic scattering data over the energy range 18–166 MeV.

Our work is organized as follows, in sect-II we introduced the theoretical formulation in sect-III we discuss the results followed by general conclusions.

2 Formalism

2.1 Cluster density

Consider a nucleus of mass number A composed of an integral number (m) of α particles, i.e., $A = 4m$. The α-cluster distribution inside the nucleus is $\rho_c(\acute{r})$, is supposed to be related to nuclear matter density distribution of the nucleus, $\rho_m(r)$, and to that of the α-particle, $\rho_\alpha(r_\alpha)$, by,

$$\rho_m(r) = \int \rho_c(\acute{r})\, \rho_\alpha(r - \acute{r}) d\vec{\acute{r}}, \quad (1)$$

This convolution relation has the following properties,

$$\langle r_m^2 \rangle = \langle r_c^2 \rangle + \langle r_\alpha^2 \rangle, \quad (2)$$

$\langle r_m^2 \rangle$, $\langle r_c^2 \rangle$ and $\langle r_\alpha^2 \rangle$ are the mean square radius for the matter, cluster and α-particle densities, respectively. Both $\langle r_m^2 \rangle$ and $\langle r_\alpha^2 \rangle$ are known experimentally. For $\langle r_\alpha^2 \rangle$ there are two important reported values, $1.47 \pm 0.02\, fm$ obtained from elastic electron scattering [28,29] and the other $1.58 \pm 0.04\, fm$ extracted from Glauber model [30,31] for the analysis of the experimental interaction cross sections. In this work we adopted the value $1.47 \pm 0.02\, fm$ to be consistent with the ref. [16].

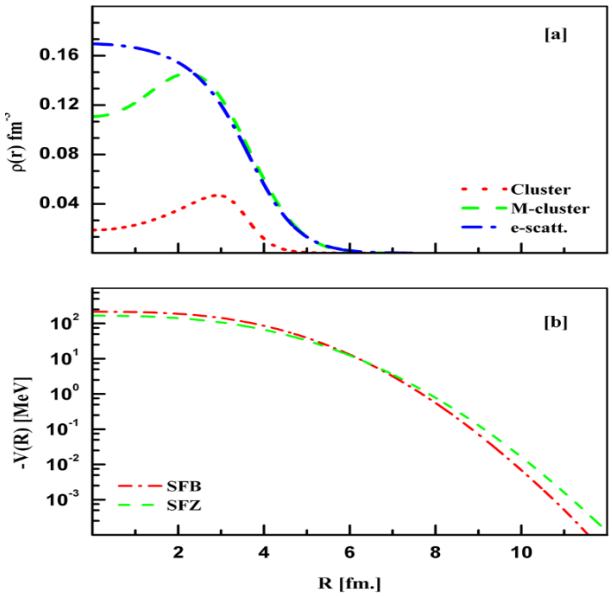

Fig. 1: [a] This figure presents the calculated α-cluster density (dot line), the matter based on the cluster density (dashed) and the electron scattering density of ^{40}Ca. [b] This figure presents the calculated cluster single folding potentials (SFC) of α-^{40}Ca system. The calculation based on α-α effective interaction of ref.[23] are shown by dashed dot line and denoted as SFB while that based on the α-α effective interaction of ref.[27] is shown by dashed line and denoted as SFZ.

The second property of convolution relation is,

$$J(\rho_m) = J(\rho_c) J(\rho_\alpha), \quad (3)$$

Where,

$$J(f) = 4\pi \int r^2 f(r) dr \quad (4)$$

$J(f)$ is the volume integral of the function $f(r)$. From these two properties (eq. (2) and eq. (3)) of the convolution relation the α-cluster density of the nucleus could be obtained using an appropriate form of $\rho_c(\acute{r})$. In this work we proposed the following three parameters Fermi form,

$$\rho_c(\acute{r}) = \rho_{0c}(1 + \omega\acute{r}^2)\left[1 + exp\left(\frac{\acute{r}-R}{a}\right)\right]^{-1} \quad (5)$$

Table 1: The calculated cluster density parameters of ^{40}Ca nucleus.

ω $[fm^2]$	R $[fm]$	a $[fm]$	$\langle r_c^2\rangle$ $[fm^2]$	$\langle r_{mc}^2\rangle$ $[fm^2]$	$\langle r_{me}^2\rangle$ $[fm^2]$
0.21955	3.47117	0.29053	9.988	12.112	12.121

This form is suggested to produce point nucleon distribution with exponential decay at the nuclear surface and a central depression expected for light nuclei after folding with the α-particle density distribution [28].

Using eq. (2) and eq. (3), We fixed the parameters of α-cluster density (eq. (5)) by varying the parameters , R and a for ^{40}Ca nucleus. The obtained parameters are listed in Table-I. In this table beside the density parameters the mean square radii $\langle r_c^2\rangle$, $\langle r_{cm}^2\rangle$ and $\langle r_{em}^2\rangle$ (cluster, point nucleon based on the present cluster, experimental, mean square radii, respectively) are tabulated in the last three columns. The obtained α-cluster density is plotted in Fig.1 [a] (dot line). Also the point nucleon density of ^{40}Ca (dashed line) obtained from the convolution of the α-cluster density and α-particle density [28] is shown in comparison with matter density obtained from electron scattering [29] (dashed dot line) in Fig.1[a].

2.2 Cluster folding model

Based on the obtained α-cluster density of ^{40}Ca and an appropriate $V_{\alpha\alpha}(s)$ α-α effective interaction, the α+^{40}Ca real optical potential could be obtained through the single folding procedure,

$$V_{SFC}(R) = \int \rho_c(r)V_{\alpha\alpha}(R - r)d\vec{r} \quad (6)$$

In this work two forms of the α-α effective interaction are used. The first is that of Buck et.al. [23]. This potential, which is also purely and strongly attractive energy-independent potential. It reproduce the energy dependence of the $l = 0, 2, 4$ and 6 on α-α scattering phase shifts reasonably well, up to about 40 MeV (lab) bombarding energy. The radial form of this potential is of the following simple Gaussian shape,

$$V_{\alpha\alpha}(r) = 122.623exp(-0.22r^2) \quad (7)$$

Using the α-cluster density parameters listed on Table-I for ^{40}Ca and α-α effective interaction (eq.7) the α-^{40}Ca real optical potential are obtained.

As another alternative a second form of the α-α effective interaction based on the single folding is used [27]. This effective interaction based on the single folding of α-nucleon density dependent effective interaction of the following,

$$\upsilon_{\alpha N}(\rho, s) = 32.3\left(1 - 0.28\rho_\alpha^{2/3}\right)exp(-0.25s^2), \quad (8)$$

With the α-particle density, $\rho_\alpha(r)$ of the following simple Gaussian shape [28],

$$\rho_\alpha(r) = 0.4229exp(-0.7024r^2), \quad (9)$$

The obtained α-α effective interaction using eq. (6) through eq. (9), has the following general form,

$$V_{\alpha\alpha}(r) = V_A(r) + V_R(r), \quad (10)$$

Where,

$$V_A(r) = \upsilon_0 \int \rho_\alpha(r_\alpha)exp(-0.25s^2)d\vec{r}, \quad (11)$$

$$V_R(r) = -0.28\upsilon_0 \int \left(\rho_\alpha(r_\alpha)\right)^{5/3} exp(-0.25s^2)d\vec{r}, \qquad s = |\vec{r} - \vec{r}_\alpha|. \quad (12)$$

By performing the integration of eq. (11) and eq.(12), the α-α effective interaction (eq.(10)) takes the following explicit form,

$$V_{\alpha\alpha}(r) = 82.0\exp(-0.1844r^2) - 7.1\exp(-0.2060r^2) \quad (13),$$

Substitute eq.(7) or eq.(13) into eq.(6) the α-nucleus real part of the optical potential is obtained and the resulted real optical potentials are shown in Fig.1[b].

3 Results and Discussion

The obtained results of this work are summarized in Table-I to Table-III and in Fig.1 to Fig. 6. From Table-I it is shown the mean square radius for ^{40}Ca point nucleon density obtained in this work are in a good agreement with the experimental one [29].

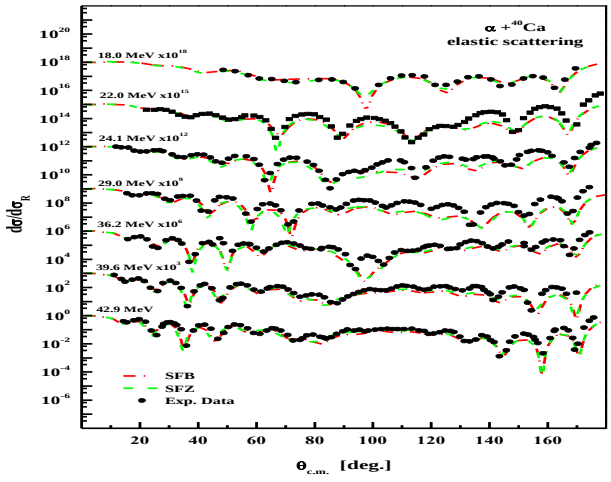

Fig. 1: This figure presents the calculated elastic scattering cross section based on the SFB and SFZ potentials for the energy between 18 and 42.9 MeV. the calculations

based on SFB potential are shown by dashed dot lines and denoted as SFB while the calculations based on SFZ potential are shown by dashed lines and denoted as SFZ.

From Fig.1 [a] it is shown that the obtained point nucleon density has an exponential tail and quite agrees with the experimental density profile in the surface region and does not agree at the central region where the obtained density has large depression. We implemented the obtained α-

Table 2: Optical model fitting parameters of the system α+^{40}Ca elastic scattering using real SFB potential

E [MeV]	Nr	Wi [MeV]	Jr [$MeV.fm^3$]	Ji [$MeV.fm^3$]	σ_R [$mb.$]
18.0	1.050	12.731	434.34	46.07	1110.0
22.0	1.061	14.391	438.97	52.07	1220.0
24.1	1.066	14.754	440.83	53.39	1258.0
29.0	1.032	17.810	427.09	64.45	1322.0
36.2	1.361	20.634	563.01	74.66	1433.0
39.6	1.049	19.970	433.93	72.26	1390.0
42.9	1.085	20.345	448.93	73.62	1406.0
46.0	1.083	21.300	448.13	77.07	1416.0
48.0	1.075	22.534	444.74	81.54	1423.0
49.5	1.080	23.425	446.95	84.76	1431.0
50.0	0.760	24.150	314.39	87.38	1381.0
54.0	0.754	20.258	311.90	73.30	1354.0
58.0	0.749	21.351	309.83	77.26	1362.0
61.0	0.744	21.280	307.74	76.94	1360.0
62.0	0.750	22.007	310.20	79.63	1367.0
81.0	0.712	25.964	294.60	93.95	1383.0
100.0	0.696	27.136	287.96	98.19	1376.0
104.0	0.892	39.587	369.08	143.24	1482.0
141.7	0.650	26.048	268.88	94.25	1323.0
166.0	0.608	24.255	251.51	87.76	1277.0

cluster density of ^{40}Ca in the single folding procedure to generate the real part of the optical model potential. The calculated potentials are denoted as SFB for α-α effective interaction based on eq. (7) and denoted as SFZ for α-α effective interaction based on eq. (13). The calculated potential are presented in Fig.1 [b]. It is shown from this figure that the SFB and SFZ potentials intersect each other at around 6 *fm* and SFZ potential is deeper than SFB potential for distance larger than 6 *fm* and the situation is reversed for distance less than 6 *fm*. This due to introduction of a repulsive part in the α-α effective interaction.

The auto-search computer code HIOPTM-94[36] is feed with the two calculated potential individually to analyze the elastic scattering data of α+^{40}Ca system. These calculated potentials are considered as the real part of the general ion-ion potential,

$$U(R) = V_c(R) - N_r V_{SFC}(R) - iW_0[f(R)]^n \qquad (14)$$

N_r is a normalization factor, $V_c(R)$ is the Coulomb potential of a charged spheres with radius $R_C = 1.3A_T^{1/3}$ and $f(R)$ is the radial form factor of the imaginary potential which is usually chosen in the form of Woods Saxon,

$$f(R) = [1 + \exp(R - R_i/a_i)]^{-1} \qquad (15)$$

W_0, R_i and a_i are the depth, the half radius and diffuseness parameters of the imaginary, respectively. Since the system under study is characterized by the low absorption of α-particle a power $n \geq n$ is needed ($n = 2$ in this work). A search on nuclear potential parameters are carried out to get best fitting to experimental data by minimizing χ^2 , which is defined as

$$\chi^2 = \frac{1}{N}\sum_{i=1}^{N}\left(\frac{\sigma_{cal}(\theta_i)-\sigma_{exp}(\theta_i)}{\Delta\sigma_{exp}(\theta_i)}\right)^2. \qquad (16)$$

Where $\sigma_{cal}(\theta_i)$ and $\sigma_{exp}(\theta_i)$ are the calculated and experimental cross sections, respectively, at angle, θ_i $\Delta\sigma_{exp}(\theta_i)$ is the experimental error and N is the number of data points.

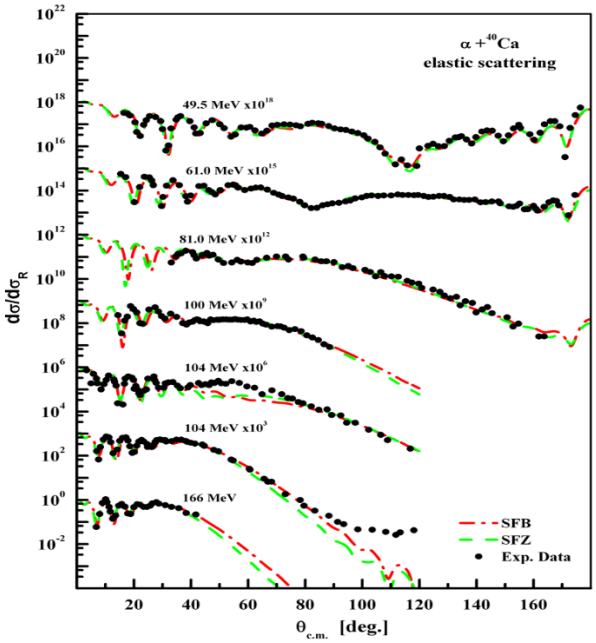

Fig. 2: The same as Fig.2 but for the energy range between 49.5 and 166 MeV.

The experimental data at this energy range are taken from ref. [33] and references therein. The search is carried out on two fitting parameters, namely the real normalization factor and the depth parameter of square Woods Saxon imaginary potential. We found an imaginary potential of

fixed shape parameters ($R_i = 1.686\,fm$ and $a_i = 1.061\,fm$ for SFB potential, and $R_i = 1.758\,fm$ and $a_i = 1.142\,fm$ for SFZ potential) is able to reproduce successfully the experimental data. The best resulted parameters of the elastic scattering calculations are listed on Table-II for the calculations based on SFB and Table-III for the calculations based on SFZ potential. The resulted elastic scattering cross sections are shown in comparison with experimental data on Fig.2-4. The results based on SFB potential are shown by dashed-dot lines while the results based on SFZ potential are shown by dashed lines on these figures.

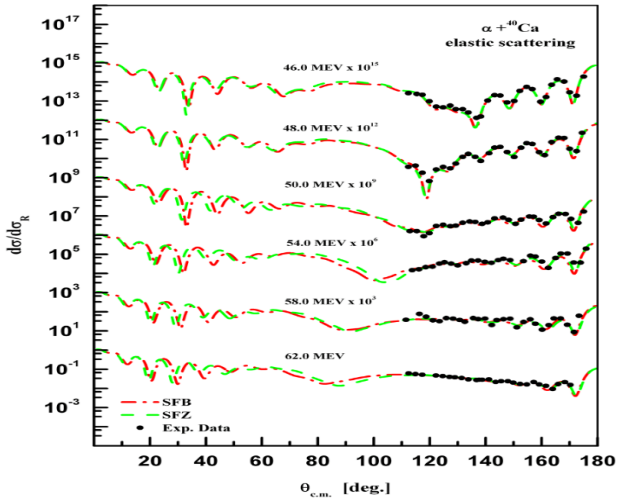

Fig. 3: The same as Fig.-2 but for backward scattering data at energy range between 50 and 62 MeV.

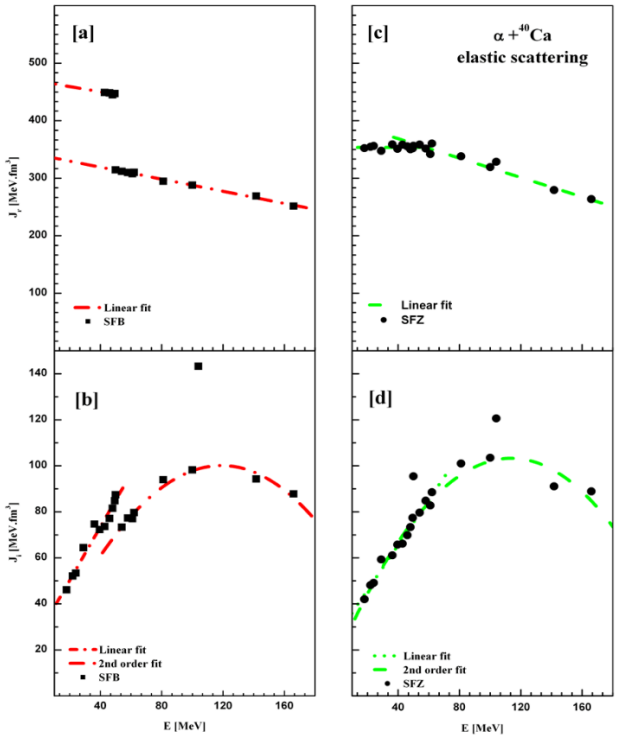

Fig. 4 : This figure presents the energy dependence of the volume integrals of the SFB and SFZ potential and the volume integrals of the squared Woods Saxon imaginary potentials.

Table 3: Optical model fitting parameters of the system α+^{40}Ca elastic scattering using real SFZ potential

E $[MeV]$	Nr	Wi $[MeV]$	Jr $[MeV.fm^3]$	Ji $[MeV.fm^3]$	σ_R $[mb.]$
18.0	1.057	10.275	352.24	42.03	1178.
22.0	1.064	11.759	354.56	48.10	1286.
24.1	1.068	12.010	356.10	49.13	1323.
29.0	1.043	14.494	347.61	59.30	1390.
36.2	1.077	14.944	358.89	61.14	1438.
39.6	1.053	16.064	351.14	65.72	1453.
42.9	1.075	16.175	358.42	66.17	1464.
46.0	1.066	17.083	355.39	69.88	1474.
48.0	1.050	17.930	350.19	73.35	1481.
49.5	1.055	18.923	351.84	77.41	1493.
50.0	1.069	23.326	356.31	95.42	1534.
54.0	1.075	19.472	358.50	79.66	1502.
58.0	1.055	20.737	351.55	84.83	1510.
61.0	1.026	20.228	342.11	82.79	1500.
62.0	1.081	21.644	360.35	88.54	1521.
81.0	1.014	24.691	338.16	101.01	1528.
100.0	0.958	25.304	319.35	103.51	1509.
104.0	0.794	29.474	328.53	120.57	1533.
141.7	0.838	22.268	279.43	91.10	1415.
166.0	0.791	21.732	263.59	88.90	1378.

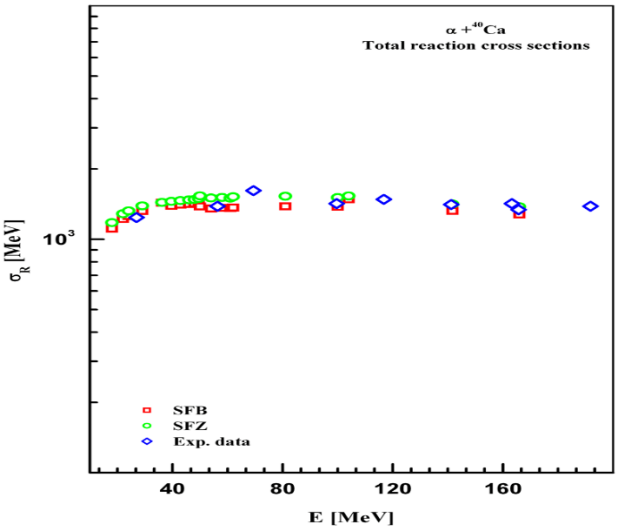

Fig. 5 : SFB and SFZ potential calculated reaction cross section in comparison with experimental data.

From the figures it is shown the calculated real potential is succeed in reproducing the data at 18 MeV. For energies above 18 MeV and below 42.9 MeV the two potential successes to reproduce the data for angles up to 80°. Also it is shown as the energy increase above 29 MeV the success of the calculated potentials to reproduce the data increase and become in a good agreement with the data for energies above 42.9 MeV. This could be attribute to two reasons 1-) the strong coupling effect to the elastic scattering channel 2-) the alpha cluster structure is not suitable for low energies and the ideal alpha structure could

occur only for incident or excitation energy above 40 MeV. Since this failure at low energy region is common to any optical model potentials, see refs. [32-35], we expect the coupling effect has the major effect. So for this energy region a generalized optical potential with dispersive correction is needed to analyze the data.

In general it is found from Table -II and Table-III that the obtained real and imaginary volume integrals show clear energy dependence as shown on Fig.5 [a] to Fig.5 [d]. Fig.5 [a] represents the energy dependence of the real SFB potential. From this figure it is shown that the energy dependence for energy below 50 MeV is different from that of energy above 50 MeV. This energy dependence could be represented by the following linear relations,

$$J_r^{SFB} = 468.42275 - 0.45569\,E, \qquad 42.9 \le E \le 49.5 \qquad (17)$$

$$J_r^{SFB} = 340.37425 - 0.52521\,E, \qquad 50.0 \le E \le 166 \qquad (18)$$

This is clear from the different normalization factor at these two energy range. Fig.5 [b] is represented the energy dependence of the imaginary volume integrals conjugate to the SFB potential. As it is shown from the figure, the energy dependence for energy below 50 is different from that above as well as the case of the real one. The energy dependence for the low energy region could be represented by the following relation,

$$J_i^{SFB} = 27.03559 + 1.15934\,E, \qquad 18 \le E < 50 \qquad (19)$$

For the energy above 50 MeV the energy dependence could be represented by a 2nd order equation as follows,

$$J_i^{SFB} = 10.67756 + 1.50554\,E - 0.00633\,E^2, \qquad 54 \le E \le 166 \qquad (20)$$

The energy dependence of the SFZ volume integrals are shown in Fig.5[c]. From this figure it is shown the energy dependence has very weak energy dependence for energy between 18 and 50 MeV. This energy dependence could be represented by the following linear relation,

$$J_r^{SFZ} = 353.57621 + 0.00174\,E, \qquad 18 \le E \le 50 \qquad (21)$$

For higher energies the volume integrals has a linear decreasing energy dependence of the form,

$$J_r^{SFZ} = 402.31907 - 0.84209\,E, \qquad 50 \le E \le 166 \qquad (22)$$

The imaginary volume integrals conjugated to the SFZ real potential also has clear energy dependence. If the energy range between 18 and 62 MeV is considered the imaginary volume integrals could be represented by the following linear relation,

$$J_i^{SFZ} = 26.26589 + 0.98311\,E, \qquad 18 \le E \le 62 \qquad (23)$$

If the whole energy range is considered the variation of the volume, integrals with energy could be represented by the following 2nd order equation,

$$J_i^{SFZ} = 16.73846 + 1.52844\,E - 0.00673\,E^2, \qquad 18 \le E \le 166 \qquad (24)$$

The energy dependence of the reaction cross section σ_R obtained from the present analysis of the α-^{40}Ca reactions compared with experimental ones is demonstrated in Fig. [6]. From this figure it is shown the agreement of the calculated reaction cross sections obtained using the SFB and SFZ potentials with the experimental data [33]. The existence of the total reaction (absorption) cross section σ_R beside the elastic scattering angular distribution are added another dimension for the investigation of the success and validity of our α-cluster model.

In conclusion we found that the simple model of α-cluster presented in this work is reasonably reproduced the point nucleon density of ^{40}Ca at the surface region where the elastic scattering is sensitive. Also we found that the α-cluster single folding model used in the present work works well in the description of α+^{40}Ca scattering. The obtained single folded real potentials reasonably reproduced the experimental data over a wide range of energy (above 40 MeV) and angular distributions. This success reflects the success and validity of our model independent α-cluster model for energy above 40 MeV while for energies below 40 MeV our α-cluster model is still doubtful. Also we found the appropriate choice of the effective α-α interaction affects the results of the calculation. That means a more realistic effective α-α interaction incorporate energy and density dependent for α+α system is probably needed for a good description of α+nucleus scattering in the base of any α-cluster model. We found that the absorption of α in the α+^{40}Ca scattering is peaked at energy around 120 MeV.

Finally the present work the present analysis shows the ability of the model independent α-cluster model to reproduce the measured elastic α+^{40}Ca scattering and reaction cross sections through the broad energy range especially for energies above 40 MeV. This success motivated us to refine this model by minimizing the binding energy of the ^{40}Ca nucleus using any energy density functional formula. In addition it motivated us to use this model for the elastic scattering of other α-conjugate nuclei and for other reactions at different energies.

References

[1] S.Watanabe, Nucl. Phys. **8,** 484 (1958).

[2] G.R. Satchler, W.G. Love, Phys. Rep. **55,** 183 (1979).

[3] M.E. Brandan, G.R. Satchler, Phys. Rep. **285,** 143 (1997).

[4] T. Furumoto and Y. Sakuragi: Phys. Rev. **C 74,** 034606 (2006).

[5] Dao T. Khoa, W. vonOertzen, H.G. Bohlen, F. Nuoffer Nucl. Phys. **A** 672, 387 (2000); Dao T. Khoa, Phys. Rev. C

63, 034007 (2001).

[6] S. Ohkubo, Y. Hirabayashi, Journal of Physics: Conference Series **11**, 012014 (2008).

[7] Wei Zou, Yuan Tian, and Zhong-Yu Ma, Phys. Rev. C 78, 064613 (2008).

[8] T. L. Belyaeva, A. N. Danilov, A. S. Demyanova, S. A. Goncharov, A. A. Ogloblin, and R. Perez-Torres, Phys. Rev. C 82, 054618 (2010).

[9] Y. Hirabayashi and S. Ohkubo, Phys. Rev C 88, 014314 (2013);

[10] Yong-Xu Yang, Qing-Run Li, Nucl. Phys. **A** 732, 3 (2004).

[11] Yong-Xu Yang, Hai-Lan Tan, and Qing-Run Li, Phys. Rev C 82, 024607 (2010).

[12] M. A. Hassanain, CHINESE J.Phys. 49, NO.2, 589(2011).

[13] M.N.A. Abdullah, M.S.I. Sarker, S. Hossain, S.K. Das, A.S.B. Tariq, M.A. Uddin, A.S. Mondal, A.K. Basak, S. Ali, H.M. Sen Gupta , F.B. Malik, Phys. Lett. **B 571,** 45 (2003).

[14] P. Schuck , Y. Funaki , H. Horiuchi , G. Ropke , A. Tohsaki , T. Yamada , Progress in Particle and Nuclear Physics **59**, 285 (2007).

[15] M. Asai, K. Tsukada, S. Ichikawa, M. Sakama, H. Haba, I. Nishinaka, Y. Nagame, S. Goto, Y. Kojima, Y. Oura, and M. Shibata, Phys. Rev. **C 73,** 067301 (2006).

[16] M.El-Azab Farid, Z.M.M.Mahmoud, and G.S.Hassan, Nucl. Phys. **A 691,** 671 (2001).

[17] M.El-Azab Farid, Z.M.M.Mahmoud, and G.S.Hassan, Phys. Rev. **C 64,** 014310 (2001).

[18] M.A.Hassanain, Awad A.Ibraheem, and M.El-Azab Farid, Phys. Rev. **C 77**, 034601 (2008).

[19] M.A.Hassanain, Awad A.Ibraheem, Shikha M.M. Al Sebiey, S.R. Mokhtar, M.A. Zaki, Zakaria M.M. Mahmoud, K.O. Behairy, and M.El-Azab Farid, Phys. Rev. **C 87,** 064606 (2013).

[20] M. Karakoc and I. Boztosun, Phys. Rev. C 73, 047601 (2006), Int. J. Mod. Phys. **E 15**, 1317 (2006).

[21] V. G. Neudatchin, V. I. Kukulin, V. L. Korotkikh, and V. P. Korennoy,Phys. Lett. **B 34,** 581 (1971).

[22] L. Marquez: Phys. Rev. **C 28,** 2525 (1983).

[23] B. Buck, H. Friedrich, and C. Wheathly: Nucl. Phys. **A 275,** 246 (1977).

[24] P. Darriulat, G. Igo, H. G. Pugh, and H. D. Holmgren: Phys. Rev. **137** (1965) B315.

[25] M. Avrigeanu, W. von Oertzen, A.J.M. Plompen, V. Avrigeanu, Nucl. Phys. **A723,** 104 (2003).

[26] M. El-Azab Farid, Phys. Rev. **C74,** 064616 (2006).

[27] Zakaria M. M. Mahmoud, Awad A. Ibranheen, and M. El-Azab Farid, J. Phys. Soc. JPN, **81,** 124201 (2012).

[28] J. S. McCarthy, I. Sick, and R. R. Whitney: Phys. Rev. **C 15,** 1396 (1977).

[29] H. De Vries, C. W. De Jager, and C. De Vries: At. Data Nucl. Data Tables **36,** 495 (1987).

[30] J. S. Al-Khalili, J. A. Tostevin, and I. J. Thompson: Phys. Rev. **C 54,** 1843 (1996).

[31] O. M. Knyaz'kov, I. N. Kuchtina, and A. Fayans: Phys. Part. Nucl. **30,** 369 (1999).

[32] Th. Delbar, Gh. Grgoire, G. Paic, R. Ceuleneer, F. Michel, R. Vanderpoorten, R. Budzanowski, H. Dabrowski, L. Friendl, K. Grotoski, S. Micek, R. Planeta, A. Strzalkowski, A. Eberhard, Phys. Rev. **C18,** 1237 (1978).

[33] M.N.A. Abdullah, A.B. Idris, A.S.B. Tariq, M.S. Islama, S.K. Das, M.A. Uddina, A.S. Mondal, A.K. Basak, I. Reichstein , H.M. Sen Guptad, F.B. Malik, Nucl. Phys. **A760**, 40 (2005).

[34] Ashok Kumar, S. Kailas, Sarla Rathi, K. Mahata, Nucl. Phys. **A776**, 105 (2006).

[35] B. Back, J. C. Johnston, A. C. Merchant and S. M. Perez, Phys. Rev. **C52**, 1840 (1995).

[36] N.M. Clarke; private communication.